

Projector-based efficient estimation of force constants

Atsuto Seko^{1,*} and Atsushi Togo²

¹*Department of Materials Science and Engineering, Kyoto University, Kyoto 606-8501, Japan*

²*Center for Basic Research on Materials National Institute for Materials Science, Tsukuba, Ibaraki 305-0047, Japan*

(Dated: March 7, 2024)

Estimating force constants for crystal structures is a fundamental aspect of calculating various phonon-related properties. However, it can be a challenging task, particularly when dealing with a large number of atoms or when third and higher-order force constants are needed. In this study, we propose an efficient approach that involves constructing a complete orthonormal basis set of the force constants. We formulate this approach using projector matrices and their eigenvectors corresponding to the requirements for the force constants. This basis set allows us to infer the force constants from displacement-force datasets precisely. Our efficient algorithms for the basis-set construction and force constant estimation from a displacement-force dataset are implemented in the `symfc` code [1]. Furthermore, several applications are demonstrated in this study, indicating that the current approach helps to obtain force constants efficiently and precisely.

I. INTRODUCTION

Force constants of crystal structures play a crucial role in calculating various phonon-related properties [2–4]. To estimate these force constants, we typically use supercell approaches in conjunction with the finite displacement method [5–9]. Moreover, in self-consistent phonon approaches, effective force constants are often determined from supercell structures that replicate the atomic distribution at a specific temperature [10, 11]. In these approaches, random or systematic atomic displacements are introduced into supercells. The forces acting on atoms in the supercells are calculated, and then supercell force constants are estimated from the dataset composed of the displacements and forces. However, determining the force-constant elements necessitates numerous supercells with different configurations of displacements because the force-constant elements that need to be determined are plentiful.

The force-constant elements that need to be determined can be reduced into a basis set for representing the force constants by applying permutation symmetry rules, which are derived from the definition of the force constants as the derivatives of the potential energy, and sum rules, which are derived from the invariance with infinitesimal translations [3]. In addition, symmetric properties of the structure can also reduce the force-constant elements [7, 8, 12]. A significantly reduced but complete orthonormal basis set allows for efficient and precise calculation of force constants that meet all the requirements for the force constants [13, 14]. However, constructing the basis set and estimating the force constants using the basis set can be computationally demanding, especially when dealing with many atoms or when third and higher-order force constants are needed.

Various approaches have been developed to estimate force constants precisely using compressed sensing, as

reported in the literature [15, 16]. Although there are other approaches available [6–8], the force constant estimation remains computationally challenging. In this study, we propose a projector-based efficient approach that involves constructing a complete orthonormal basis set of force constants. We introduce several compression techniques that allow the basis set to be efficiently reduced. These techniques compress a projection matrix using eigenvectors of another projection matrix onto subspaces defined by partial requirements for the force constants. We have implemented the current procedures for efficient basis-set construction and force constant estimation from a displacement-force dataset in the `symfc` code [1]. We also demonstrate various applications of the current approach, indicating that it leads to obtaining force constants efficiently and precisely.

II. FORMULATION OF PROJECTION MATRICES

A. Crystal potential and force constants

Force constants of a crystal are derived from the Taylor expansion of the potential energy \mathcal{V} with respect to atomic displacements. In this study, we consider supercell force constants, which are estimated from a set of finite displacements and forces acting on atoms in supercells. For a supercell with N atoms, the potential energy is represented by

$$\begin{aligned} \mathcal{V} = & \Theta_0 + \sum_{i,\alpha} \Theta_{i\alpha} u_{i\alpha} \\ & + \frac{1}{2} \sum_{i\alpha,j\beta} \Theta_{i\alpha,j\beta} u_{i\alpha} u_{j\beta} \\ & + \frac{1}{3!} \sum_{i\alpha,j\beta,k\gamma} \Theta_{i\alpha,j\beta,k\gamma} u_{i\alpha} u_{j\beta} u_{k\gamma} \\ & + \dots, \end{aligned} \quad (1)$$

* seko@cms.mtl.kyoto-u.ac.jp

where i, j , and k are the atomic indices within the supercell, and α, β , and γ are the Cartesian components. The second-order and third-order supercell force constants are represented by $\Theta_{i\alpha,j\beta}$ and $\Theta_{i\alpha,j\beta,k\gamma}$, respectively. In addition, we assume that the first-order force constants $\Theta_{i\alpha}$ is equal to zero because atomic displacements are measured from their equilibrium positions.

B. Projection matrix for second-order force constants

In the current formulation, the second-order force constants are represented in a column vector form with $9N^2$ elements as

$$\boldsymbol{\theta}^{(\text{FC2})} = [\Theta_{1x,1x}, \Theta_{1x,1y}, \Theta_{1x,1z}, \Theta_{1x,2x}, \dots]^\top, \quad (2)$$

which are listed in the ascending order of (i, α, j, β) . We start by considering force constants that are invariant with space group operations \mathcal{G} for the target structure. As we are discussing supercell force constants, the lattice translation subgroup in \mathcal{G} is limited to those of the lattice points inside the supercell. An operation $\hat{g} \in \mathcal{G}$ acts on the force constant vector as

$$\hat{g}\boldsymbol{\theta}^{(\text{FC2})} = \boldsymbol{\theta}^{(\text{FC2})} [\boldsymbol{\Gamma}(\hat{g}) \otimes \boldsymbol{\Gamma}(\hat{g})], \quad (3)$$

where $\boldsymbol{\Gamma}(\hat{g})$ denotes the matrix representation of operation \hat{g} for the first-order force constants $\{\Theta_{i\alpha}\}$. We use the group-theoretical projection operator method [13] to reduce the Kronecker product of representations to the identity irreducible representation. The projection matrix for the identity irreducible representation is given as

$$\mathbf{P}_{\text{spg}} = \frac{1}{|\mathcal{G}|} \sum_{\hat{g} \in \mathcal{G}} \boldsymbol{\Gamma}(\hat{g}) \otimes \boldsymbol{\Gamma}(\hat{g}), \quad (4)$$

where $|\mathcal{G}|$ denotes the order of group \mathcal{G} .

Then, we introduce projection matrices onto force constants that satisfy the sum rules and permutation symmetry rules. The sum rule for $(i\alpha, \beta)$ and the permutation symmetry rule for $(i\alpha, j\beta)$ are expressed as

$$\sum_j \Theta_{i\alpha,j\beta} = 0 \quad (5)$$

and

$$\Theta_{i\alpha,j\beta} - \Theta_{j\beta,i\alpha} = 0, \quad (6)$$

respectively. These rules are independent linear constraints for the force constants. We can represent them in a matrix form as $\mathbf{C}^\top \boldsymbol{\theta}^{(\text{FC2})} = 0$. Therefore, a force-constant basis set that satisfies these linear constraints spans the complementary subspace of the kernel of \mathbf{C}^\top [17]. The kernel of \mathbf{C}^\top is written as

$$\text{Ker}(\mathbf{C}^\top) = \{\boldsymbol{\theta}^{(\text{FC2})} \in \mathbb{R}^{9N^2} | \mathbf{C}^\top \boldsymbol{\theta}^{(\text{FC2})} = 0\}, \quad (7)$$

and the orthogonal projection matrix onto the complementary subspace of $\text{Ker}(\mathbf{C}^\top)$ is given by [17, 18]

$$\mathbf{P}_{\text{perm} \cap \text{sum}} = \mathbf{I} - \mathbf{C}(\mathbf{C}^\top \mathbf{C})^{-1} \mathbf{C}^\top, \quad (8)$$

where \mathbf{I} denotes the unit matrix of size $9N^2$.

The column unit vector $\mathbf{v}_{i\alpha\beta}$ represents the sum rule for (i, α, β) , which can be expressed as $\mathbf{v}_{i\alpha\beta}^\top \boldsymbol{\theta}^{(\text{FC2})} = 0$, in accordance with Eq. (5). This means that the vector $\mathbf{v}_{i\alpha\beta}$ has only N non-zero elements. Moreover, the set of vectors $\{\mathbf{v}_{i\alpha\beta}\}$ are mutually orthonormal. Similarly, the column unit vector $\mathbf{w}_{i\alpha,j\beta}$ describes the permutation symmetry rule for the combination of $i\alpha$ and $j\beta$ as $\mathbf{w}_{i\alpha,j\beta}^\top \boldsymbol{\theta}^{(\text{FC2})} = 0$. Therefore, the vector $\mathbf{w}_{i\alpha,j\beta}$ has only two non-zero elements, which are $1/\sqrt{2}$ and $-1/\sqrt{2}$. Additionally, the set of vectors $\{\mathbf{w}_{i\alpha,j\beta}\}$, with $i\alpha < j\beta$ in the lexicographic order, is orthonormal.

Using the complete set of $\mathbf{v}_{i\alpha\beta}$ and $\mathbf{w}_{i\alpha,j\beta}$, matrix \mathbf{C} is described as

$$\mathbf{C} = [\mathbf{C}_v, \mathbf{C}_w], \quad (9)$$

where

$$\mathbf{C}_v = [\dots, \mathbf{v}_{i\alpha\beta}, \dots], \quad \mathbf{C}_w = [\dots, \mathbf{w}_{i\alpha,j\beta}, \dots]. \quad (10)$$

Note that two vectors $\mathbf{v}_{i\alpha\beta}$ and $\mathbf{w}_{i\alpha,j\beta}$ are linearly independent, without necessarily being orthogonal. Therefore, the projection matrix onto the complementary subspace of $\text{Ker}(\mathbf{C}^\top)$ requires an inverse matrix computation as given by Eq. (8).

Finally, we present the full projection matrix onto the intersection of vector subspaces determined by projection matrices \mathbf{P}_{spg} and $\mathbf{P}_{\text{perm} \cap \text{sum}}$. Since projection matrices \mathbf{P}_{spg} and $\mathbf{P}_{\text{perm} \cap \text{sum}}$ are commutative as shown in the Appendix B, the full projection matrix can be written as $\mathbf{P} = \mathbf{P}_{\text{spg}} \mathbf{P}_{\text{perm} \cap \text{sum}}$ [17, 19]. By solving the eigenvalue problem for the full projection matrix, i.e.,

$$\mathbf{P}\mathbf{b} = \mathbf{b}, \quad (11)$$

we can obtain an orthonormal basis set for representing force constants. This basis set is invariant with space group operations and satisfies the sum rules and permutation symmetry rules. Since all non-zero eigenvalues of the projection matrix are one, the number of independent basis vectors is equal to the trace of the projection matrix.

C. Projection matrix for third-order force constants

Third-order force constants are represented in a vector form with $27N^3$ elements as

$$\boldsymbol{\theta}^{(\text{FC3})} = [\Theta_{1x,1x,1x}, \Theta_{1x,1x,1y}, \Theta_{1x,1x,1z}, \Theta_{1x,1x,2x}, \dots]^\top, \quad (12)$$

which are listed in the ascending order of $(i, \alpha, j, \beta, k, \gamma)$. An operation $\hat{g} \in \mathcal{G}$ acts on the third-order force constant vector as

$$\hat{g}\boldsymbol{\theta}^{(\text{FC3})} = \boldsymbol{\theta}^{(\text{FC3})} [\boldsymbol{\Gamma}(\hat{g}) \otimes \boldsymbol{\Gamma}(\hat{g}) \otimes \boldsymbol{\Gamma}(\hat{g})]. \quad (13)$$

Therefore, the projection matrix for the identity irreducible representation is given as

$$\mathbf{P}_{\text{spg}} = \frac{1}{|\mathcal{G}|} \sum_{\hat{g} \in \mathcal{G}} \boldsymbol{\Gamma}(\hat{g}) \otimes \boldsymbol{\Gamma}(\hat{g}) \otimes \boldsymbol{\Gamma}(\hat{g}). \quad (14)$$

The sum rules and permutation symmetry rules can also be represented in a matrix form as $\mathbf{C}^\top \boldsymbol{\theta}^{(\text{FC3})} = 0$, which is the same as the representation of the rules used for second-order force constants. The kernel of \mathbf{C}^\top is written as

$$\text{Ker}(\mathbf{C}^\top) = \{\boldsymbol{\theta}^{(\text{FC3})} \in \mathbb{R}^{27N^3} | \mathbf{C}^\top \boldsymbol{\theta}^{(\text{FC3})} = 0\}, \quad (15)$$

and the orthogonal projection matrix onto the complementary subspace of $\text{Ker}(\mathbf{C}^\top)$ is given by [17, 18]

$$\mathbf{P}_{\text{perm} \cap \text{sum}} = \mathbf{I} - \mathbf{C}(\mathbf{C}^\top \mathbf{C})^{-1} \mathbf{C}^\top, \quad (16)$$

where \mathbf{I} denotes the unit matrix of size $27N^3$.

The sum rule for $(i, \alpha, j, \beta, \gamma)$ is written as

$$\sum_k \Theta_{i\alpha, j\beta, k\gamma} = 0, \quad (17)$$

hence, column unit vector $\mathbf{v}_{i\alpha j\beta\gamma}$ represents the sum rule for $(i, \alpha, j, \beta, \gamma)$, which can be expressed as $\mathbf{v}_{i\alpha j\beta\gamma}^\top \boldsymbol{\theta}^{(\text{FC3})} = 0$. The vector $\mathbf{v}_{i\alpha j\beta\gamma}$ has only N non-zero elements among $27N^3$ elements, and the set of vectors $\{\mathbf{v}_{i\alpha j\beta\gamma}\}$ are mutually orthonormal.

Representing the permutation symmetry rules is more complicated than applied to the second-order force constants. The permutation symmetry rule for $(i\alpha, j\beta, k\gamma)$ is expressed as

$$\begin{aligned} \Theta_{i\alpha, j\beta, k\gamma} - \Theta_{i\alpha, k\gamma, j\beta} &= 0 \\ \Theta_{i\alpha, j\beta, k\gamma} - \Theta_{j\beta, i\alpha, k\gamma} &= 0 \\ \Theta_{i\alpha, j\beta, k\gamma} - \Theta_{j\beta, k\gamma, i\alpha} &= 0 \\ \Theta_{i\alpha, j\beta, k\gamma} - \Theta_{k\gamma, i\alpha, j\beta} &= 0 \\ \Theta_{i\alpha, j\beta, k\gamma} - \Theta_{k\gamma, j\beta, i\alpha} &= 0, \end{aligned} \quad (18)$$

when all three indices $i\alpha, j\beta$, and $k\gamma$ are different. These equations can be described by a matrix composed of the column unit vectors $\mathbf{W}_{i\alpha, j\beta, k\gamma}$ as $\mathbf{W}_{i\alpha, j\beta, k\gamma}^\top \boldsymbol{\theta}^{(\text{FC3})} = 0$. Each column vector of the matrix $\mathbf{W}_{i\alpha, j\beta, k\gamma}$ has two non-zero elements, which are $1/\sqrt{2}$ and $-1/\sqrt{2}$. The column vectors are not orthogonal but linearly independent. The permutation symmetry rule for $(i\alpha, i\alpha, k\gamma)$ is given as

$$\begin{aligned} \Theta_{i\alpha, i\alpha, k\gamma} - \Theta_{i\alpha, k\gamma, i\alpha} &= 0 \\ \Theta_{i\alpha, i\alpha, k\gamma} - \Theta_{k\gamma, i\alpha, i\alpha} &= 0. \end{aligned} \quad (19)$$

In this case, the matrix composed of column unit vectors $\mathbf{W}_{i\alpha, i\alpha, k\gamma}$ is also written as $\mathbf{W}_{i\alpha, i\alpha, k\gamma}^\top \boldsymbol{\theta}^{(\text{FC3})} = 0$, where

each column vector has two non-zero elements, which are $1/\sqrt{2}$ and $-1/\sqrt{2}$.

Using a linearly-independent complete set of $\mathbf{v}_{i\alpha j\beta\gamma}$ and $\mathbf{W}_{i\alpha, j\beta, k\gamma}$, matrix \mathbf{C} is described as

$$\mathbf{C} = [\mathbf{C}_v, \mathbf{C}_w], \quad (20)$$

where

$$\mathbf{C}_v = [\cdots, \mathbf{v}_{i\alpha j\beta\gamma}, \cdots], \quad \mathbf{C}_w = [\cdots, \mathbf{W}_{i\alpha, j\beta, k\gamma}, \cdots]. \quad (21)$$

Finally, the full projection matrix is given as $\mathbf{P} = \mathbf{P}_{\text{spg}} \mathbf{P}_{\text{perm} \cap \text{sum}}$ [17, 19]. By solving the eigenvalue problem for the full projection matrix, $\mathbf{P}\mathbf{b} = \mathbf{b}$, an orthonormal basis set for representing third-order force constants is obtained.

III. EFFICIENT BASIS SET CONSTRUCTION

A. Decomposition of projection matrix

To efficiently obtain the projection matrix of $\mathbf{P}_{\text{perm} \cap \text{sum}}$ and formulate a more efficient procedure, we use an approximate projection matrix instead of computing the inverse of $\mathbf{C}^\top \mathbf{C}$, which can be computationally prohibitive. This involves considering individual projection matrices for the sum rules and permutation symmetry rules. For the second-order force constants, orthogonal projection matrices \mathbf{P}_v and \mathbf{P}_w onto the complementary subspaces of $\text{Ker}(\mathbf{C}_v^\top)$ and $\text{Ker}(\mathbf{C}_w^\top)$ are expressed using orthonormal vector sets $\{\mathbf{v}_{i\alpha\beta}\}$ and $\{\mathbf{w}_{i\alpha, j\beta}\}$ as [18]

$$\begin{aligned} \mathbf{P}_v &= \mathbf{I} - \sum_{i=1}^N \sum_{\alpha=1}^3 \sum_{\beta=1}^3 \mathbf{v}_{i\alpha\beta} \mathbf{v}_{i\alpha\beta}^\top \\ &= \mathbf{I} - \mathbf{C}_v \mathbf{C}_v^\top \end{aligned} \quad (22)$$

and

$$\begin{aligned} \mathbf{P}_w &= \mathbf{I} - \sum_{(i\alpha, j\beta)} \mathbf{w}_{i\alpha, j\beta} \mathbf{w}_{i\alpha, j\beta}^\top \\ &= \mathbf{I} - \mathbf{C}_w \mathbf{C}_w^\top, \end{aligned} \quad (23)$$

respectively. For the third-order force constants, orthogonal projection matrices \mathbf{P}_v and \mathbf{P}_w onto the complementary subspaces of $\text{Ker}(\mathbf{C}_v^\top)$ and $\text{Ker}(\mathbf{C}_w^\top)$ are given as

$$\begin{aligned} \mathbf{P}_v &= \mathbf{I} - \sum_{i=1}^N \sum_{\alpha=1}^3 \sum_{j=1}^N \sum_{\beta=1}^3 \sum_{\gamma=1}^3 \mathbf{v}_{i\alpha j\beta\gamma} \mathbf{v}_{i\alpha j\beta\gamma}^\top \\ &= \mathbf{I} - \mathbf{C}_v \mathbf{C}_v^\top \end{aligned} \quad (24)$$

and

$$\mathbf{P}_w = \mathbf{I} - \mathbf{C}_w (\mathbf{C}_w^\top \mathbf{C}_w)^{-1} \mathbf{C}_w^\top, \quad (25)$$

respectively.

Using the non-commutative matrices \mathbf{P}_v and \mathbf{P}_w , the projection matrix $\mathbf{P}_{\text{perm}\cap\text{sum}}$ is expressed using the von Neumann–Halperin theorem as [19–22]

$$\mathbf{P}_{\text{perm}\cap\text{sum}} = \lim_{p \rightarrow \infty} \mathbf{P}_w (\mathbf{P}_v \mathbf{P}_w)^p. \quad (26)$$

To obtain an approximation of the projection matrix $\mathbf{P}_{\text{perm}\cap\text{sum}}$, a finite value of p can be used. However, the matrix product $\mathbf{P}_{\text{perm}\cap\text{sum}} \simeq \mathbf{P}_w (\mathbf{P}_v \mathbf{P}_w)^1$, i.e., $p = 1$, suffices to derive a basis set for the full projection matrix. By solving the eigenvalue problem of the approximated full projection matrix given as

$$\tilde{\mathbf{P}} = \mathbf{P}_{\text{spg}} \mathbf{P}_w \mathbf{P}_v \mathbf{P}_w \quad (27)$$

and removing its eigenvectors with eigenvalues less than one, we can obtain the basis set for the full projection matrix.

B. Matrix compression

When computing the product of two large projection matrices of size $(9N^2, 9N^2)$ for the second order or $(27N^3, 27N^3)$ for the third order, it can be computationally expensive. To avoid allocating large matrices and computing the products of large matrices, we use a compression technique that involves the eigenvalue decomposition of projection matrices. In the eigenvalue decomposition, a projection matrix \mathbf{P}_i is decomposed by its eigenvectors \mathbf{B}_i as

$$\mathbf{P}_i = \mathbf{B}_i \mathbf{B}_i^\top, \quad (28)$$

where \mathbf{B}_i is of size $(9N^2, n_i)$ or $(27N^3, n_i)$. If the eigenvectors of the projection matrix are well-compressed, sparse, and efficiently obtained, they can be helpful in compressing large matrices.

Let us consider the case where product $\mathbf{P}_j \mathbf{P}_i \mathbf{P}_j$ can be included in a product representation of the full projection matrix. If \mathbf{P}_i and \mathbf{P}_j are commutative, i.e., $[\mathbf{P}_i, \mathbf{P}_j] = 0$, product $\mathbf{P}_j \mathbf{P}_i \mathbf{P}_j$ is equal to $\mathbf{P}_i \mathbf{P}_j$ as

$$\mathbf{P}_j \mathbf{P}_i \mathbf{P}_j = \mathbf{P}_i \mathbf{P}_j^2 = \mathbf{P}_i \mathbf{P}_j, \quad (29)$$

which is derived using the idempotent property of the projection matrix, $\mathbf{P}_j^2 = \mathbf{P}_j$. When eigenvectors of \mathbf{P}_j , \mathbf{B}_j , are known and well compressed, \mathbf{P}_i may be efficiently compressed by \mathbf{B}_j , as

$$\begin{aligned} \mathbf{P}_j \mathbf{P}_i \mathbf{P}_j &= \mathbf{B}_j \mathbf{B}_j^\top \mathbf{P}_i \mathbf{B}_j \mathbf{B}_j^\top \quad (\mathbf{P}_j = \mathbf{B}_j \mathbf{B}_j^\top) \\ &= \mathbf{B}_j \mathbf{P}_{i\downarrow j} \mathbf{B}_j^\top, \end{aligned} \quad (30)$$

where $\mathbf{P}_{i\downarrow j}$ denotes the compressed matrix of \mathbf{P}_i by basis set \mathbf{B}_j as

$$\mathbf{P}_{i\downarrow j} = \mathbf{B}_j^\top \mathbf{P}_i \mathbf{B}_j. \quad (31)$$

Using this compression, the eigenvectors of $\mathbf{P}_j \mathbf{P}_i \mathbf{P}_j$ can be efficiently calculated as follows. (1) If eigenvectors of

$\mathbf{P}_i = \mathbf{B}_i \mathbf{B}_i^\top$ are derived without constructing \mathbf{P}_i and solving the eigenvalue problem for \mathbf{P}_i as shown below, $\mathbf{P}_{i\downarrow j}$ is written as

$$\mathbf{P}_{i\downarrow j} = \mathbf{B}_j^\top \mathbf{B}_i \mathbf{B}_i^\top \mathbf{B}_j. \quad (32)$$

In general, the size of $\mathbf{B}_j^\top \mathbf{B}_i$ is small, so we firstly compute $\mathbf{A} = \mathbf{B}_j^\top \mathbf{B}_i$, and then compute $\mathbf{P}_{i\downarrow j} = \mathbf{A} \mathbf{A}^\top$. If it is necessary to construct \mathbf{P}_i , we compute $\mathbf{P}_{i\downarrow j}$ using Eq. (31). (2) The eigenvalue problem of compressed projection matrix $\mathbf{P}_{i\downarrow j}$ is solved as $\mathbf{P}_{i\downarrow j} = \mathbf{B}_{i\downarrow j} \mathbf{B}_{i\downarrow j}^\top$, where $\mathbf{B}_{i\downarrow j}$ is the compressed eigenvectors by \mathbf{B}_j . (3) The eigenvectors of $\mathbf{P}_j \mathbf{P}_i \mathbf{P}_j$, $\mathbf{B}_{i\cdot j}$, is derived as

$$\mathbf{B}_{i\cdot j} = \mathbf{B}_j \mathbf{B}_{i\downarrow j}, \quad (33)$$

and $\mathbf{P}_j \mathbf{P}_i \mathbf{P}_j$ is rewritten by

$$\begin{aligned} \mathbf{P}_j \mathbf{P}_i \mathbf{P}_j &= \mathbf{B}_{i\cdot j} \mathbf{B}_{i\cdot j}^\top \\ &= \mathbf{B}_j \mathbf{B}_{i\downarrow j} \mathbf{B}_{i\downarrow j}^\top \mathbf{B}_j^\top. \end{aligned} \quad (34)$$

This matrix compression procedure is frequently used in the reduction of the full projection matrix as shown below.

C. Application of sum rules

We utilize the equation of $\mathbf{P}_v = \mathbf{I} - \mathbf{C}_v \mathbf{C}_v^\top$, which is presented in Eqs. (22) and (24), to reduce the full projection matrix by the sum rules. This method is efficient because both the unit matrix and \mathbf{C}_v are sparse matrices. On the other hand, the eigenvectors of \mathbf{P}_v , \mathbf{B}_v , typically contains a larger number of non-zero elements than \mathbf{C}_v .

D. Application of permutation symmetry rules

The eigenvectors of the projection matrix onto the complementary space of $\text{Ker}(\mathbf{C}_w^\top)$, \mathbf{P}_w , can be efficiently obtained without actually constructing the projection matrix \mathbf{P}_w . These eigenvectors form a basis for the vector space that satisfies the permutation symmetry rules. For the second order, the permutation symmetry rule for $(i\alpha, j\beta)$ is given by Eq. (23), and is represented by a single vector $\mathbf{w}_{i\alpha, j\beta}$ as $\mathbf{w}_{i\alpha, j\beta}^\top \boldsymbol{\theta} = 0$. Because the set of vectors $\{\mathbf{w}_{i\alpha, j\beta}\}$ is orthonormal, the vector $\mathbf{w}_{i\alpha, j\beta}^\perp$ orthogonal to $\mathbf{w}_{i\alpha, j\beta}$ can be an eigenvector of \mathbf{P}_w , which has only two non-zero elements of $1/\sqrt{2}$ for columns (i, α, j, β) and (j, β, i, α) . If $i\alpha = j\beta$, no permutation symmetry rules should be considered. Therefore, $\mathbf{w}_{i\alpha, i\alpha}^\perp$ can be defined as the vector that has only a non-zero element of one for column (i, α, i, α) . Thus, the eigenvectors of \mathbf{P}_w , \mathbf{B}_w , is written as

$$\mathbf{B}_w = [\cdots, \mathbf{w}_{i\alpha, j\beta}^\perp, \cdots]^\top, \quad (35)$$

where vectors $\{\mathbf{w}_{i\alpha, j\beta}^\perp\}$ are also mutually orthonormal. The size of \mathbf{B}_w is $(9N^2, n_w)$, where $n_w \simeq 9N^2/2$. The

number of non-zero elements is $9N^2$ in \mathbf{B}_w , which is much smaller than the total number of elements in \mathbf{B}_w .

For the third order, the permutation symmetry rule for $(i\alpha, j\beta, k\gamma)$ can be found in Eq. (18), which consists of five equations. These equations are represented in a matrix form as $\mathbf{W}_{i\alpha, j\beta, k\gamma}^\top \boldsymbol{\theta} = 0$, and the submatrix of $\mathbf{W}_{i\alpha, j\beta, k\gamma}$ that includes only non-zero rows is given as

$$\mathbf{W}_{i\alpha, j\beta, k\gamma} = \frac{1}{\sqrt{2}} \begin{bmatrix} 1 & 1 & 1 & 1 & 1 \\ -1 & 0 & 0 & 0 & 0 \\ 0 & -1 & 0 & 0 & 0 \\ 0 & 0 & -1 & 0 & 0 \\ 0 & 0 & 0 & -1 & 0 \\ 0 & 0 & 0 & 0 & -1 \end{bmatrix}. \quad (36)$$

Therefore, the column vector $\mathbf{w}_{i\alpha, j\beta, k\gamma}^\perp$, which is orthonormal to all column vectors of $\mathbf{W}_{i\alpha, j\beta, k\gamma}$, can be considered as an eigenvector of \mathbf{P}_w . It is obtained as

$$\mathbf{w}_{i\alpha, j\beta, k\gamma}^\perp = \frac{1}{\sqrt{6}} [1 \ 1 \ 1 \ 1 \ 1]^\top, \quad (37)$$

which is expressed in the submatrix representation by omitting zero elements. If $i\alpha = j\beta$ and $i\alpha \neq k\gamma$, the permutation symmetry rule for $(i\alpha, i\alpha, k\gamma)$ is given by Eq. (19). The two equations in Eq. (19) are also represented as $\mathbf{W}_{i\alpha, i\alpha, k\gamma}^\top \boldsymbol{\theta} = 0$, where the submatrix of $\mathbf{W}_{i\alpha, i\alpha, k\gamma}$ that includes only non-zero rows is expressed as

$$\mathbf{W}_{i\alpha, i\alpha, k\gamma} = \frac{1}{\sqrt{2}} \begin{bmatrix} 1 & 1 \\ -1 & 0 \\ 0 & -1 \end{bmatrix}. \quad (38)$$

Therefore, the vector orthonormal to all column vectors of $\mathbf{W}_{i\alpha, j\beta, k\gamma}$, $\mathbf{w}_{i\alpha, i\alpha, k\gamma}^\perp$, is given as

$$\mathbf{w}_{i\alpha, i\alpha, k\gamma}^\perp = \frac{1}{\sqrt{3}} [1 \ 1 \ 1]^\top. \quad (39)$$

If $i\alpha = j\beta$ and $i\alpha = k\gamma$, there exist no permutation symmetry rules. Therefore, vector $\mathbf{w}_{i\alpha, i\alpha, i\alpha}^\perp$ is defined as the vector that has only a non-zero element of one for column $(i, \alpha, i, \alpha, i, \alpha)$. Thus, the eigenvectors of \mathbf{P}_w , \mathbf{B}_w , is written as

$$\mathbf{B}_w = [\cdots, \mathbf{w}_{i\alpha, j\beta, k\gamma}^\perp, \cdots]^\top, \quad (40)$$

where vectors $\mathbf{w}_{i\alpha, j\beta, k\gamma}^\perp$ are also mutually orthonormal. The size of \mathbf{B}_w is $(27N^3, n_w)$, where $n_w \simeq 27N^3/6$. The number of non-zero elements is $27N^3$ in \mathbf{B}_w , which is much smaller than the total number of elements in \mathbf{B}_w .

E. Effective use of lattice translation group

Here, we are introducing the projection matrix for the identity irreducible representation of the lattice translation group, which is a normal subgroup of the space group. Although the projection matrix for the lattice

translation group is not mandatory for describing the full projection matrix, it can help in compressing projection matrices that are made up of the full projection matrix. The projection matrix for the lattice translation group can be formulated in a similar way to the derivation of the projection matrix for the permutation symmetry rules.

The force constants remain constant for operations in lattice translation group $\mathcal{T} = \{t_1, t_2, \cdots\}$, which are also included in group \mathcal{G} . We identify representative atoms using indices $\{i'\}$ and express the translation of atom i as $t_n(i)$. For the second-order force constants of paired atoms, which include a representative atom i' , the invariant property is expressed as

$$\Theta_{i'\alpha, j\beta} - \Theta_{t_n(i')\alpha, t_n(j)\beta} = 0, \quad (41)$$

where operation t_n is not the identity. Therefore, $|\mathcal{T}| - 1$ equations for each (i', α, j, β) are represented in a matrix form of $\mathbf{T}_{i'\alpha, j\beta}$ as $\mathbf{T}_{i'\alpha, j\beta}^\top \boldsymbol{\theta} = 0$. The submatrix of $\mathbf{T}_{i'\alpha, j\beta}$ composed only of non-zero rows is expressed as

$$\mathbf{T}_{i'\alpha, j\beta} = \frac{1}{\sqrt{2}} \begin{bmatrix} 1 & 1 & 1 & 1 \\ -1 & 0 & 0 & 0 \\ 0 & -1 & 0 & 0 \\ 0 & 0 & -1 & 0 \\ 0 & 0 & 0 & -1 \\ \vdots & & & \ddots \end{bmatrix}, \quad (42)$$

where the submatrix is of size $(|\mathcal{T}|, |\mathcal{T}| - 1)$. The vector orthonormal to all column vectors of $\mathbf{T}_{i'\alpha, j\beta}$ can be an eigenvector of \mathbf{P}_{LT} given in the submatrix representation as

$$\mathbf{t}_{i'\alpha, j\beta}^\perp = \frac{1}{\sqrt{|\mathcal{T}|}} [1 \ 1 \ 1 \ \cdots]^\top. \quad (43)$$

The eigenvectors of \mathbf{P}_{LT} , \mathbf{B}_{LT} , is then described as

$$\mathbf{B}_{\text{LT}} = [\cdots, \mathbf{t}_{i'\alpha, j\beta}^\perp, \cdots]^\top, \quad (44)$$

where vectors $\{\mathbf{t}_{i'\alpha, j\beta}^\perp\}$ are also mutually orthonormal. The size of \mathbf{B}_{LT} is $(9N^2, 9N^2/|\mathcal{T}|)$. The number of non-zero elements is $9N^2$ in \mathbf{B}_{LT} , hence, \mathbf{B}_{LT} is a sparse matrix.

The third-order force constants for triplet atoms, including a representative atom i' , are also invariant with respect to operations in \mathcal{T} . This is described as

$$\Theta_{i'\alpha, j\beta, k\gamma} - \Theta_{t_n(i')\alpha, t_n(j)\beta, t_n(k)\gamma} = 0, \quad (45)$$

where operation t_n is not the identity. Similar to the second-order force constants, $|\mathcal{T}| - 1$ equations for each $(i', \alpha, j, \beta, k, \gamma)$ are represented in a matrix form of $\mathbf{T}_{i'\alpha, j\beta, k\gamma}$ as $\mathbf{T}_{i'\alpha, j\beta, k\gamma}^\top \boldsymbol{\theta}^{(\text{FC3})} = 0$. Therefore, the submatrix forms of $\mathbf{T}_{i'\alpha, j\beta, k\gamma}$ and $\mathbf{t}_{i'\alpha, j\beta, k\gamma}^\perp$ are obtained by replacing indices $(i', j\beta)$ with indices $(i'\alpha, j\beta, k\gamma)$ in Eqs. (42) and (43). Thus, the eigenvectors of \mathbf{P}_{LT} is written as

$$\mathbf{B}_{\text{LT}} = [\cdots, \mathbf{t}_{i'\alpha, j\beta, k\gamma}^\perp, \cdots]^\top, \quad (46)$$

where vectors $\{t_{i\alpha,j\beta,k\gamma}^\perp\}$ are also mutually orthonormal. The size of \mathbf{B}_{LT} is $(27N^3, 27N^3/|\mathcal{T}|)$. The number of non-zero elements is $27N^3$ in \mathbf{B}_{LT} , which is much smaller than the total number of elements in \mathbf{B}_{LT} .

The projection matrix is obtained from the eigenvectors as $\mathbf{P}_{\text{LT}} = \mathbf{B}_{\text{LT}}\mathbf{B}_{\text{LT}}^\top$. The projection matrix has the relationship with \mathbf{P}_{spg} of

$$\mathbf{P}_{\text{LT}}\mathbf{P}_{\text{spg}} = \mathbf{P}_{\text{spg}}\mathbf{P}_{\text{LT}} = \mathbf{P}_{\text{spg}}, \quad (47)$$

because $t_n\mathcal{G} = \mathcal{G}$ for any operation $t_n \in \mathcal{T}$ that is also included in group \mathcal{G} , $t_n \in \mathcal{G}$. Therefore, the projection matrix for the lattice translation group leaves \mathbf{P}_{spg} invariant.

F. Properties of projection matrices

The commutation relations between projection matrices are significant in building force-constant basis sets in an efficient manner. These relations include

$$[\mathbf{P}_{\text{spg}}, \mathbf{P}_v] = 0, [\mathbf{P}_{\text{spg}}, \mathbf{P}_w] = 0, [\mathbf{P}_v, \mathbf{P}_w] \neq 0. \quad (48)$$

The commutation relations on the projection matrix for the lattice translation group are also useful in compressing projection matrices in addition to the relationship of Eq. (47). They are given as

$$[\mathbf{P}_{\text{LT}}, \mathbf{P}_v] = 0, [\mathbf{P}_{\text{LT}}, \mathbf{P}_w] = 0. \quad (49)$$

In addition, these projection matrices are idempotent and orthogonal, which are represented by

$$\mathbf{P}_{\text{spg}}^2 = \mathbf{P}_{\text{spg}}, \mathbf{P}_v^2 = \mathbf{P}_v, \mathbf{P}_w^2 = \mathbf{P}_w, \mathbf{P}_{\text{LT}}^2 = \mathbf{P}_{\text{LT}} \quad (50)$$

and

$$\mathbf{P}_{\text{spg}}^\top = \mathbf{P}_{\text{spg}}, \mathbf{P}_v^\top = \mathbf{P}_v, \mathbf{P}_w^\top = \mathbf{P}_w, \mathbf{P}_{\text{LT}}^\top = \mathbf{P}_{\text{LT}}, \quad (51)$$

respectively.

G. Solving eigenvalue problems for projection matrices

The techniques mentioned earlier can be used to compress projection matrices. However, even in their compressed form, these matrices can still be quite extensive. Nevertheless, since they are often sparse matrices, their block-diagonal structures can be useful in solving the eigenvalue problems associated with them in an efficient manner. In this context, we are considering an orthogonal projection matrix that is represented in a block-diagonal form, which is transformed by row and column

permutations. The block-diagonal form of the orthogonal projection matrix is written as

$$\mathbf{M}^\top \mathbf{P} \mathbf{M} = \begin{bmatrix} \mathbf{I} & \mathbf{0} & \mathbf{0} \\ \mathbf{0} & \mathbf{J} & \mathbf{0} \\ \mathbf{0} & \mathbf{0} & \mathbf{K} \end{bmatrix}, \quad (52)$$

where \mathbf{M} denotes the permutation matrix for column. Submatrices \mathbf{I} , \mathbf{J} , and \mathbf{K} must all be orthogonal projection matrices so that \mathbf{P} is the orthogonal projection matrix. When we solve eigenvalue problems for the submatrices and obtain eigenvectors of \mathbf{I} , \mathbf{J} , and \mathbf{K} as

$$\mathbf{I}\mathbf{b}_I = \mathbf{b}_I, \mathbf{J}\mathbf{b}_J = \mathbf{b}_J, \mathbf{K}\mathbf{b}_K = \mathbf{b}_K, \quad (53)$$

the vectors given by

$$\mathbf{b} = \begin{bmatrix} \mathbf{b}_I \\ \mathbf{0} \\ \mathbf{0} \end{bmatrix}, \begin{bmatrix} \mathbf{0} \\ \mathbf{b}_J \\ \mathbf{0} \end{bmatrix}, \begin{bmatrix} \mathbf{0} \\ \mathbf{0} \\ \mathbf{b}_K \end{bmatrix} \quad (54)$$

can be adopted as eigenvectors of $\mathbf{M}^\top \mathbf{P} \mathbf{M}$. They are mutually orthonormal, and the trace of $\mathbf{M}^\top \mathbf{P} \mathbf{M}$ is given as

$$\text{tr}(\mathbf{M}^\top \mathbf{P} \mathbf{M}) = \text{tr}(\mathbf{I}) + \text{tr}(\mathbf{J}) + \text{tr}(\mathbf{K}), \quad (55)$$

which corresponds to the number of eigenvectors of $\mathbf{M}^\top \mathbf{P} \mathbf{M}$. Therefore, the set of eigenvectors $\{\mathbf{b}\}$ built from $\{\mathbf{b}_I\}$, $\{\mathbf{b}_J\}$, and $\{\mathbf{b}_K\}$ is complete. The eigenvectors of \mathbf{P} are finally calculated as $\mathbf{M}\mathbf{b}$.

We follow a graph-based approach to determine the permutation matrix \mathbf{M} . To achieve this, we treat the orthogonal projection matrix \mathbf{P} as an undirected graph where each row and column of the matrix corresponds to a vertex. The vertices s and t are considered adjacent only when the element of \mathbf{P} for row s and column t is non-zero. Next, we employ an efficient graph algorithm to identify the connected components [23] in the graph representation of the projection matrix. The algorithm assigns columns and rows of the projection matrix to one of the connected components, which represent block structures in the projection matrix. Finally, we construct the permutation matrix \mathbf{M} such that the columns in the same connected component are arranged adjacent to each other in the reordered projection matrix $\mathbf{M}^\top \mathbf{P} \mathbf{M}$.

H. Procedure to calculate eigenvectors of full projection matrix

The eigenvectors of the approximated projection matrix $\tilde{\mathbf{P}}$ given by Eq. (27) is calculated by following the equations shown below. We start by rewriting matrix $\tilde{\mathbf{P}}$ using the commutation relations and the idempotent properties of projection matrices as

$$\begin{aligned} \tilde{\mathbf{P}} &= \mathbf{P}_{\text{spg}}\mathbf{P}_w\mathbf{P}_v\mathbf{P}_w \\ &= \mathbf{P}_{\text{spg}}\mathbf{P}_w\mathbf{P}_v\mathbf{P}_{\text{spg}}\mathbf{P}_w. \end{aligned} \quad (56)$$

The eigenvalue decomposition of the matrix product $\mathbf{P}_{\text{spg}}\mathbf{P}_w$ is calculated as

$$\begin{aligned}
P_{\text{spg}} P_w &= P_{\text{LT}} P_{\text{spg}} P_{\text{LT}} P_w P_{\text{LT}} \\
&= B_{\text{LT}} B_{\text{LT}}^\top P_{\text{spg}} B_{\text{LT}} B_{\text{LT}}^\top B_w B_w^\top B_{\text{LT}} B_{\text{LT}}^\top \quad (P_{\text{LT}} = B_{\text{LT}} B_{\text{LT}}^\top, P_w = B_w B_w^\top) \\
&= B_{\text{LT}} P_{\text{spg}\downarrow\text{LT}} P_{w\downarrow\text{LT}} B_{\text{LT}}^\top \quad (\text{Eqs. (31) and (32)}) \\
&= B_{\text{LT}} P_{\text{spg}\downarrow\text{LT}} B_{w\downarrow\text{LT}} B_{w\downarrow\text{LT}}^\top B_{\text{LT}}^\top \quad (P_{w\downarrow\text{LT}} = B_{w\downarrow\text{LT}} B_{w\downarrow\text{LT}}^\top) \\
&= B_{\text{LT}} (B_{w\downarrow\text{LT}} B_{w\downarrow\text{LT}}^\top) P_{\text{spg}\downarrow\text{LT}} B_{w\downarrow\text{LT}} B_{w\downarrow\text{LT}}^\top B_{\text{LT}}^\top \\
&= B_{\text{LT}} B_{w\downarrow\text{LT}} P_{(\text{spg}\downarrow\text{LT})\downarrow(w\downarrow\text{LT})} B_{w\downarrow\text{LT}}^\top B_{\text{LT}}^\top \quad (\text{Eqs. (31) and (32)}) \\
&= B_{\text{LT}} B_{w\downarrow\text{LT}} B_{(\text{spg}\downarrow\text{LT})\downarrow(w\downarrow\text{LT})} B_{(\text{spg}\downarrow\text{LT})\downarrow(w\downarrow\text{LT})}^\top B_{w\downarrow\text{LT}}^\top B_{\text{LT}}^\top \\
&\quad (P_{(\text{spg}\downarrow\text{LT})\downarrow(w\downarrow\text{LT})} = B_{(\text{spg}\downarrow\text{LT})\downarrow(w\downarrow\text{LT})} B_{(\text{spg}\downarrow\text{LT})\downarrow(w\downarrow\text{LT})}^\top) \\
&= B_{\text{spg}\cap w} B_{\text{spg}\cap w}^\top,
\end{aligned} \tag{57}$$

where

$$B_{\text{spg}\cap w} = B_{\text{LT}} B_{w\downarrow\text{LT}} B_{(\text{spg}\downarrow\text{LT})\downarrow(w\downarrow\text{LT})}. \tag{58}$$

Then, the eigenvalue decomposition of matrix \tilde{P} is computed by

$$\begin{aligned}
\tilde{P} &= P_{\text{spg}} P_w P_v P_{\text{spg}} P_w \\
&= B_{\text{spg}\cap w} B_{\text{spg}\cap w}^\top P_v B_{\text{spg}\cap w} B_{\text{spg}\cap w}^\top \\
&= B_{\text{spg}\cap w} P_{v\downarrow(\text{spg}\cap w)} B_{\text{spg}\cap w}^\top \\
&= B_{\text{spg}\cap w} B_{v\downarrow(\text{spg}\cap w)} B_{v\downarrow(\text{spg}\cap w)}^\top B_{\text{spg}\cap w}^\top \\
&= \tilde{B} \tilde{B}^\top,
\end{aligned} \tag{59}$$

where the basis set for the force constants are

$$\tilde{B} = B_{\text{spg}\cap w} B_{v\downarrow(\text{spg}\cap w)}. \tag{60}$$

Note that eigenvectors of \tilde{P} corresponding to its eigenvalues that are less than one are eliminated, as described above.

IV. FORCE CONSTANT ESTIMATION

A. Force-constant basis set expansion

The forces acting on atoms $\{f_{i\alpha}^{(s)}\}$ in a supercell structure s corresponding to atomic displacements $\{u_{i\alpha}^{(s)}\}$ can be simply written as

$$f_{i\alpha}^{(s)} = - \sum_{j\beta} \Theta_{i\alpha,j\beta} u_{j\beta}^{(s)} - \frac{1}{2} \sum_{j\beta} \sum_{k\gamma} \Theta_{i\alpha,j\beta,k\gamma} u_{j\beta}^{(s)} u_{k\gamma}^{(s)} + \dots \tag{61}$$

The force constants are expanded in basis sets given by Eq. (60) as

$$\begin{aligned}
\Theta_{i\alpha,j\beta} &= \sum_b w_b^{(\text{FC2})} \tilde{B}_{i\alpha,j\beta,b}^{(\text{FC2})} \\
&= \sum_b w_b^{(\text{FC2})} \left[\sum_c C_{i\alpha,j\beta,c}^{(\text{FC2})} E_{c,b}^{(\text{FC2})} \right]
\end{aligned} \tag{62}$$

and

$$\begin{aligned}
\Theta_{i\alpha,j\beta,k\gamma} &= \sum_b w_b^{(\text{FC3})} \tilde{B}_{i\alpha,j\beta,k\gamma,b}^{(\text{FC3})} \\
&= \sum_b w_b^{(\text{FC3})} \left[\sum_c C_{i\alpha,j\beta,k\gamma,c}^{(\text{FC3})} E_{c,b}^{(\text{FC3})} \right],
\end{aligned} \tag{63}$$

where w_b denotes the expansion coefficient for b -th basis. Here, the symbols $B_{\text{spg}\cap w}$ and $B_{v\downarrow(\text{spg}\cap w)}$ shown in Eq. (60) are abbreviated as C and E , respectively. Then, the forces in structure s are expressed as

$$\begin{aligned}
f_{i\alpha}^{(s)} &= - \sum_b w_b^{(\text{FC2})} \sum_{j\beta} \sum_c u_{j\beta}^{(s)} C_{i\alpha,j\beta,c}^{(\text{FC2})} E_{c,b}^{(\text{FC2})} \\
&\quad - \frac{1}{2} \sum_b w_b^{(\text{FC3})} \sum_{j\beta} \sum_{k\gamma} \sum_c u_{j\beta}^{(s)} u_{k\gamma}^{(s)} C_{i\alpha,j\beta,k\gamma,c}^{(\text{FC3})} E_{c,b}^{(\text{FC3})} \\
&\quad + \dots
\end{aligned} \tag{64}$$

Therefore, the forces are rewritten as

$$f_{i\alpha}^{(s)} = \sum_b w_b^{(\text{FC2})} x_{i\alpha,b}^{(s,\text{FC2})} + \sum_b w_b^{(\text{FC3})} x_{i\alpha,b}^{(s,\text{FC3})} + \dots \tag{65}$$

where

$$x_{i\alpha,b}^{(s,\text{FC2})} = - \sum_{j\beta} \sum_c u_{j\beta}^{(s)} C_{i\alpha,j\beta,c}^{(\text{FC2})} E_{c,b}^{(\text{FC2})} \tag{66}$$

and

$$x_{i\alpha,b}^{(s,\text{FC3})} = - \frac{1}{2} \sum_{j\beta} \sum_{k\gamma} \sum_c u_{j\beta}^{(s)} u_{k\gamma}^{(s)} C_{i\alpha,j\beta,k\gamma,c}^{(\text{FC3})} E_{c,b}^{(\text{FC3})}. \tag{67}$$

The forces in structure s are also expressed in a matrix form by considering the force constants up to the third order as

$$\mathbf{f}^{(s)} = \mathbf{X}^{(s)} \mathbf{w}, \tag{68}$$

where

$$\mathbf{f}^{(s)} = \begin{bmatrix} \vdots \\ f_{i\alpha}^{(s)} \\ \vdots \end{bmatrix}, \tag{69}$$

$$\begin{aligned} \mathbf{X}^{(s)} &= [\mathbf{X}^{(s,FC2)} \quad \mathbf{X}^{(s,FC3)}] \\ &= \begin{bmatrix} \dots & \vdots & \dots & \vdots & \dots \\ \dots & x_{i\alpha,b}^{(s,FC2)} & \dots & x_{i\alpha,b}^{(s,FC3)} & \dots \\ \dots & \vdots & \dots & \vdots & \dots \end{bmatrix}, \end{aligned} \quad (70)$$

and

$$\mathbf{w} = \begin{bmatrix} \mathbf{w}^{(FC2)} \\ \mathbf{w}^{(FC3)} \end{bmatrix} = \begin{bmatrix} \vdots \\ w_b^{(FC2)} \\ \vdots \\ w_b^{(FC3)} \\ \vdots \end{bmatrix}. \quad (71)$$

B. Force constant estimation

The expansion coefficients \mathbf{w} are determined from the forces acting on atoms in N_s structures, which correspond to the displacement set, using standard linear regression. The training dataset is expressed in a matrix form as

$$\mathbf{X} = \begin{bmatrix} \mathbf{X}^{(1)} \\ \mathbf{X}^{(2)} \\ \mathbf{X}^{(3)} \\ \vdots \\ \mathbf{X}^{(N_s)} \end{bmatrix}, \quad \mathbf{y} = \begin{bmatrix} \mathbf{f}^{(1)} \\ \mathbf{f}^{(2)} \\ \mathbf{f}^{(3)} \\ \vdots \\ \mathbf{f}^{(N_s)} \end{bmatrix}, \quad (72)$$

and the solution for the coefficients \mathbf{w} is given by

$$\mathbf{w} = (\mathbf{X}^\top \mathbf{X})^{-1} \mathbf{X}^\top \mathbf{y}. \quad (73)$$

The force constants can then be recovered from the coefficients \mathbf{w} as

$$\begin{aligned} \boldsymbol{\theta}^{(FC2)} &= \mathbf{C}^{(FC2)} \mathbf{E}^{(FC2)} \mathbf{w}^{(FC2)} \\ \boldsymbol{\theta}^{(FC3)} &= \mathbf{C}^{(FC3)} \mathbf{E}^{(FC3)} \mathbf{w}^{(FC3)}. \end{aligned} \quad (74)$$

However, computing matrix \mathbf{X} can be a resource-intensive process, especially when dealing with large displacement-force datasets and basis sets. To optimize memory allocation and efficiently estimate expansion coefficients, we employ a technique from the recursive method for linear regression. We begin by considering the normal equation in linear regression, $\mathbf{X}^\top \mathbf{X} \mathbf{w} = \mathbf{X}^\top \mathbf{y}$. When the dataset is divided into n_q subsets, $\mathbf{X}^\top \mathbf{X}$ and $\mathbf{X}^\top \mathbf{y}$ can be calculated as

$$\mathbf{X}^\top \mathbf{X} = \sum_{q=1}^{n_q} \mathbf{X}_q^\top \mathbf{X}_q, \quad \mathbf{X}^\top \mathbf{y} = \sum_{q=1}^{n_q} \mathbf{X}_q^\top \mathbf{y}_q, \quad (75)$$

where \mathbf{X}_q and \mathbf{y}_q are q -th subsets of \mathbf{X} and \mathbf{y} , respectively. This allows us to avoid storing the entire \mathbf{X} matrix. The coefficients are obtained by solving the normal

equation with fast linear algebra libraries. When dividing the displacement-force dataset, we adopt a procedure to compute $\mathbf{X}^\top \mathbf{X}$ and $\mathbf{X}^\top \mathbf{y}$ more efficiently, which is shown in the Appendix C.

V. RESULTS AND DISCUSSION

A. Basis set construction

Given a unit cell structure and a supercell size, it is possible to efficiently calculate a basis set of second-order and third-order supercell force constants using Eqs. (57) and (59). This basis set represents supercell force constants that follow the permutational symmetry rules, sum rules, and symmetric properties of the given unit cell. Figure 1 (a) shows the size of the basis set for the second-order force constants of several crystal structures found in elemental systems. The total number of second-order force constant elements is $9N^2$, but they are significantly reduced by imposing constraints on the force constants. For the second order, we can obtain basis sets at small computational costs for supercells with up to 5000 atoms, which have approximately 10^8 force constant elements.

The total number of third-order force-constant elements is $27N^3$, which can become quite large when evaluating force constants using a typical size of supercells. However, there is an efficient procedure available that can help reduce the force constants and create orthonormal basis sets. Figures 1 (b) and (c) show the number of basis vectors for the third-order force constants of crystal structures found in elemental and ionic systems, respectively. For elemental structures, the current procedure can be used with supercells of up to 900 atoms using a common workstation, thanks to their small primitive cells and high symmetric properties. In the case of the ionic structures, the applicable numbers of atoms in supercells are reduced by decreasing lattice translations in these structures. For the well-known structures shown in Fig. 1 (c), the current procedure usually works well for supercells with up to 300 atoms. More information on the corresponding computational costs for constructing the basis sets can be found in the Appendix A.

B. Force constant evaluation

We will present four different applications of the current approach for estimating force constants. The first application involves using a machine learning potential (MLP) to calculate the lattice thermal conductivities (LTCs) in diamond Si. The second application is to calculate LTCs using the the density functional theory (DFT) calculation in diamond Si. The third application is to calculate LTCs using an MLP in wurtzite AgI. Finally, we use the DFT calculation to calculate LTCs in wurtzite-type ZnS. These applications demonstrate the

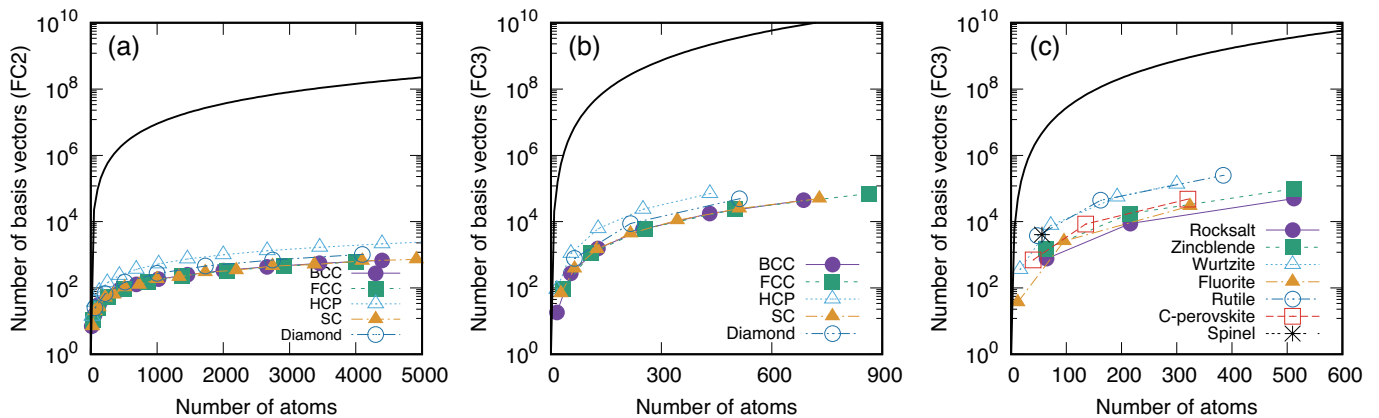


FIG. 1. (a) Number of basis vectors that completely represent second-order force constants in elemental crystal structures, i.e., the body-centered cubic (bcc), face-centered cubic (fcc), hexagonal close packed (hcp), simple cubic (sc), and diamond-type structures. Numbers of basis vectors that completely represent third-order force constants in (b) elemental crystal structures and (c) ionic crystal structures are also shown. The ionic crystal structures consist of the rocksalt, zincblende, wurtzite, fluorite, rutile, cubic perovskite (C-perovskite), and spinel structures. The black solid lines indicate the numbers of $9N^2$ and $27N^3$ for the second order and third order, respectively.

importance of choosing reasonable parameters and provide recommended settings for this approach.

1. Computational details

Supercell force constants are determined by applying standard linear regression to displacement-force datasets. A displacement-force dataset consists of N_s supercell structures that are created by introducing random atomic displacements of magnitude d into the original supercell structure with a given supercell size. The forces acting on atoms in these structures are then computed using MLPs and DFT calculations. In applications using MLPs, the forces acting on atoms in these structures are computed using polynomial MLPs [24, 25] due to their negligible computational costs in calculating force constants. The polynomial MLP represents short-range interatomic interactions with a polynomial function of polynomial invariants for arbitrary rotations. In applications using DFT calculations, force calculations were performed using the plane-wave-basis projector augmented wave method [26] within the Perdew–Burke–Ernzerhof exchange-correlation functional [27] as implemented in the VASP code [28–30].

The LTCs were calculated as the solution of the Peierls–Boltzmann equation under the relaxation time approximation [31–33] using the PHONO3PY code [34, 35]. To simplify the LTC calculations and measure the precision of force constants, only phonon-phonon scattering was considered to obtain the phonon relaxation times. The phonon lifetimes were calculated from supercell force constants as the reciprocals of the imaginary part of the phonon self-energy corresponding to the bubble diagram, which were used as the relaxation times. Phonon properties required for the LTC calculations such as phonon

group velocities and mode heat capacities were obtained from dynamical matrices derived from second-order supercell force constants. Mesh grids for sampling the reciprocal spaces are shown in each application.

2. Diamond Si (MLP)

Here, we use the same MLP as that used in the literature [36], where LTCs at grain boundaries in Si are studied using molecular dynamics simulations. This MLP is also available in the Polynomial Machine Learning Potential Repository [37], and it is estimated from a dataset with various crystal structures and their derivatives where random atomic displacements and random cell shape changes are introduced. In addition, the reciprocal spaces for the LTC calculations were sampled by the $19 \times 19 \times 19$ mesh.

The current approach based on projectors allows us to efficiently estimate force constants and LTCs for supercells with up to 512 atoms. Figure 2 shows the relationship between the LTC, the displacement magnitude, and the number of supercell structures in the displacement-force dataset. The complete basis-set sizes for the $2 \times 2 \times 2$, $3 \times 3 \times 3$, and $4 \times 4 \times 4$ supercell expansions are 777, 8800, and 49301, respectively. Therefore, the minimum numbers of supercells needed to build a full-rank predictor matrix \mathbf{X} are 5, 14, and 33, respectively. In Fig. 2 (a), it is evident that even a small number of supercells can produce precise LTCs when small displacement values are considered. Specifically, 5 and 15 supercell structures generated from random displacements with $d = 0.001 \text{ \AA}$ are sufficient to derive precise LTCs for the $2 \times 2 \times 2$ and $3 \times 3 \times 3$ expansions, respectively. Conversely, the minimal structures are not able to precisely predict the LTC when larger displacements

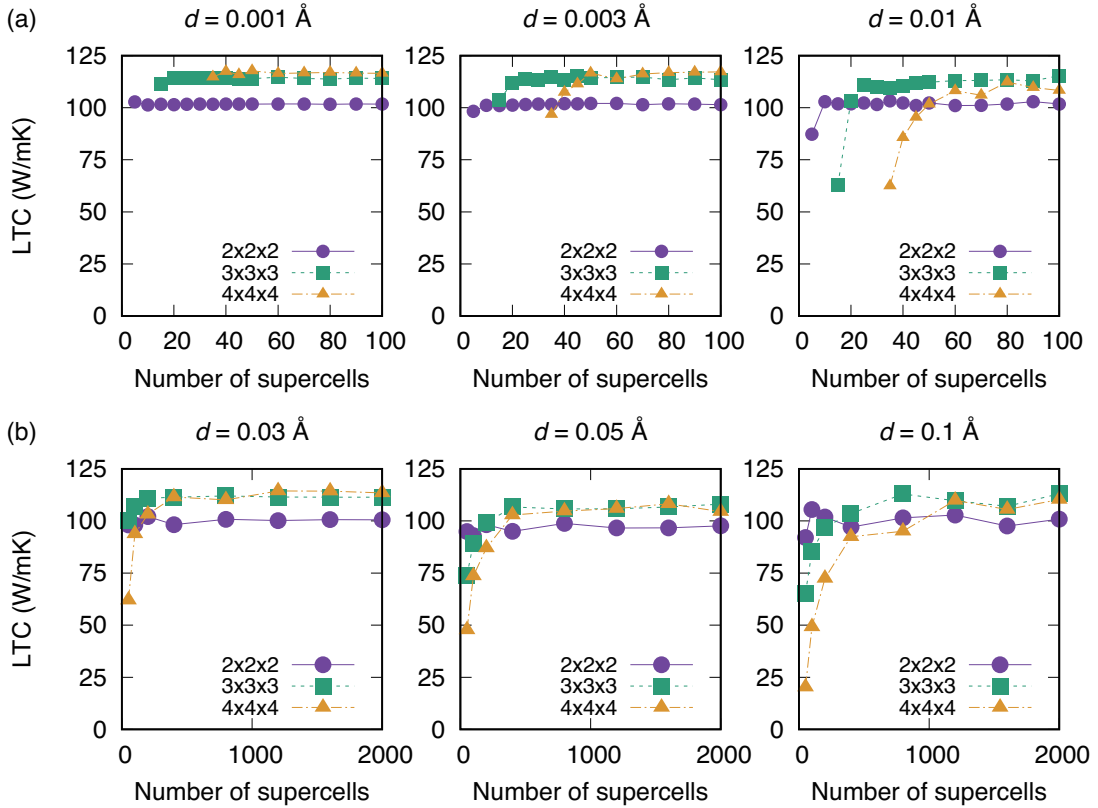


FIG. 2. (a) Relationship between the LTC and the number of supercells with $d = 0.001, 0.003,$ and 0.01 \AA in diamond Si. The minimum numbers of supercells required for constructing a full-rank predictor matrix are 5, 14, and 33 for the $2 \times 2 \times 2$, $3 \times 3 \times 3$, and $4 \times 4 \times 4$ supercell expansions, respectively. Only LTC values for the number of supercells up to 100 are shown. (b) Relationship between the LTC and the number of supercells with $d = 0.03, 0.05,$ and 0.1 \AA in diamond Si.

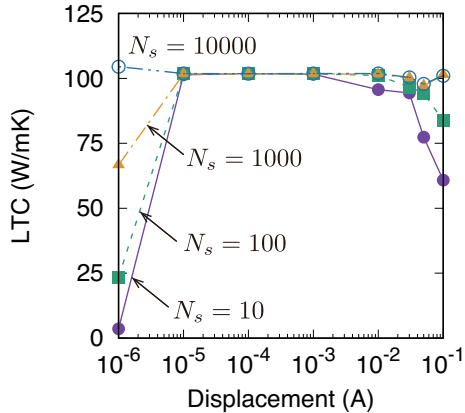


FIG. 3. Relationship between the LTC value and the magnitude of atomic displacements in diamond Si with the supercell size of $2 \times 2 \times 2$. The LTC values are calculated using displacement-force datasets composed of 10, 100, 1000, and 10000 supercell structures.

are employed. The LTC converges slowly as the number of supercells increases as can be seen in Fig. 2 (b).

Figure 3 shows the relationship between the LTC value and the magnitude of atomic displacements. When using

a quite small value of displacements, such as $d = 10^{-6} \text{ \AA}$, the forces exhibit quite small values, which leads to numerical noise becoming significant enough to contribute to force constants. As a result, many supercells are required to obtain a precise LTC. For accurate evaluation of third-order force constants without any higher-order contributions, it is better to choose the magnitude of atomic displacements within the range of 10^{-5} to 10^{-3} \AA .

Similarly, when using atomic displacements larger than 0.01 \AA , a large number of supercells are also necessary to obtain the converged LTC. This is due to the truncation errors of higher-order contributions, which make it computationally challenging to calculate the converged LTC. It is worth noting that we have utilized a constant magnitude of atomic displacements to generate each displacement-force dataset in this study. However, the current discussion is relevant to displacement-force datasets that consist of large and varying magnitudes of atomic displacements. Such datasets are found in estimating temperature-dependent force constants relevant to self-consistent phonons, which effectively contain higher-order contributions of force constants. Therefore, if self-consistent phonons are evaluated at a high temperature, we will need to use a large number of supercell structures for the displacement-force dataset.

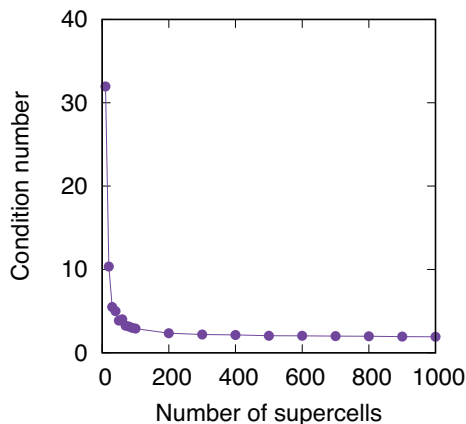


FIG. 4. Dependence of the condition number of $\mathbf{X}^T \mathbf{X}$ for the third-order force constants on the number of supercells in diamond Si. The supercell size of $2 \times 2 \times 2$ and the magnitude of atomic displacements of $d = 0.001 \text{ \AA}$ are used. The condition number is almost independent of the magnitude of atomic displacements, and similar values of the condition number can be found when using $d = 0.1 \text{ \AA}$.

The imprecise prediction of LTC is caused by errors in the forces, which are strongly related to linearly dependent relationships between predictor variables in matrix \mathbf{X} . This is known as multicollinearity, and it can make the regression coefficients sensitive to force errors. In standard linear regression, the condition number of matrix $\mathbf{X}^T \mathbf{X}$ is typically used as a measure of multicollinearity. The condition number is calculated by dividing the maximum eigenvalue of $\mathbf{X}^T \mathbf{X}$ by the minimum eigenvalue. If the condition number is significantly large, multicollinearity is likely to occur in regression.

Figure 4 shows the dependence of the condition number of matrix $\mathbf{X}^T \mathbf{X}$ for the third-order force constants with the $2 \times 2 \times 2$ supercell on the number of supercell structures. The condition number is high when using only a small number of supercells, which is close to the minimum number of supercells required for constructing a full-rank predictor matrix. This means that the prediction of LTC values is sensitive to force errors, resulting in imprecise predictions of LTC values. On the other hand, the condition number is lower at larger numbers of supercells and gradually decreases as the number of supercells increases. This behavior is consistent with the convergence patterns in LTC. Thus, by using both an orthonormal basis set for force constants and random displacements for force calculations, it is possible to create optimal conditions for estimating force constants through standard linear regression.

3. Diamond Si (DFT)

We will demonstrate an application to diamond Si, where displacement-force datasets are developed using only DFT calculations. In this application, we computed

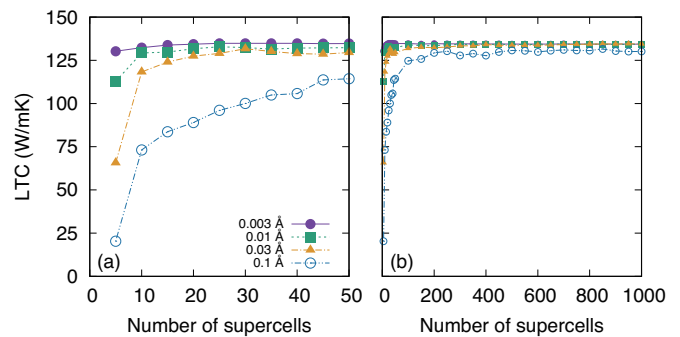


FIG. 5. (a) Relationship between the LTC and the number of supercells with $d = 0.003, 0.01, 0.03,$ and 0.1 \AA in diamond Si. Displacement-force datasets are developed using only the DFT calculation. The minimum number of supercells required for constructing a full-rank predictor matrix is five for the $2 \times 2 \times 2$ supercell expansion. Only LTC values for the number of supercells up to 50 are shown. (b) Relationship between the LTC and the number of supercells with $d = 0.003, 0.01, 0.03,$ and 0.1 \AA in diamond Si. LTC values for the number of supercells up to 1000 are shown.

the forces acting on atoms for supercell structures using DFT calculations, and used them to estimate force constants. For the DFT calculations, we constructed supercells using the $2 \times 2 \times 2$ expansion of the unit cell. The cutoff energy was set to 300 eV, and the total energies converged to less than $10^{-3} \text{ meV/supercell}$. We considered the magnitudes of atomic displacements as $d = 0.003, 0.01, 0.03,$ and 0.1 \AA .

In Fig. 5, we present the relationship between the LTC and the number of supercells in the displacement-force dataset. The LTC values obtained from the DFT calculation are slightly larger than those obtained from the polynomial MLP, as demonstrated in Ref. 36. When atomic displacements are larger than 0.01 \AA and the number of supercells is small, the LTC values are underestimated due to errors in the forces resulting from the truncation of higher-order contributions. Therefore, the minimal supercell structures fail to predict the LTC precisely.

4. Wurtzite AgI (MLP)

To calculate LTCs in wurtzite AgI, we use a polynomial MLP which was developed from a displacement-force DFT dataset using an on-the-fly approach [38]. This dataset was made up of 300 supercell structures with the magnitude of atomic displacements of 0.03 \AA . We assess the forces acting on atoms for N_s structures using the polynomial MLP, where residual forces for the calculated equilibrium atomic positions are eliminated to stabilize the LTC calculations with small atomic displacements. Additionally, we sample the reciprocal spaces for the LTC calculations using the $19 \times 19 \times 10$ mesh.

Figure 6 shows the relationship between the LTC and the number of supercells in wurtzite AgI. The supercells

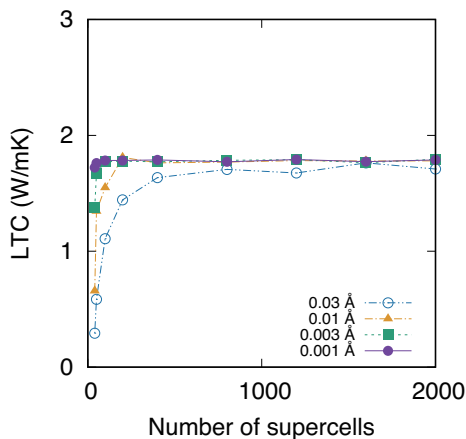


FIG. 6. Convergence behavior of LTC with respect to the number of supercells in wurtzite AgI. The supercell size is $3 \times 3 \times 2$, and the number of basis vectors for the third order force constants is 7752. The average values of diagonal elements in LTC tensors are shown.

are built using the $3 \times 3 \times 2$ expansion of the unit cell. To construct a full-rank predictor matrix \mathbf{X} , a minimum of 36 supercell structures is needed, given that the number of basis vectors for the third-order force constants is 7752. The convergence behavior of the LTC is determined by the magnitude of atomic displacements. For instance, a small number of supercell structures is sufficient to obtain a converged value of LTC for small atomic displacements, similar to the case of diamond Si. However, for large displacements, a larger number of structures are required to obtain a precise LTC value, where higher-order contributions are effectively included.

5. Wurtzite ZnS (DFT)

We are demonstrating LTC calculations using the DFT calculation in wurtzite-type ZnS. Displacement-force datasets were created using only DFT calculations. To estimate force constants, we utilized DFT calculations to compute the forces acting on atoms in supercell structures. For these calculations, we considered supercells constructed using the $3 \times 3 \times 2$ expansion of the unit cell. The cutoff energy was set to 500 eV, and the total energies converged to less than 0.001 meV/supercell. The atomic positions in the unit cell were optimized until the residual forces were less than 0.0015 eV/Å. To examine the atomic displacement dependence of the LTC, we used magnitudes of atomic displacements of $d = 0.003, 0.01, 0.03,$ and 0.1 Å.

Figure 7 shows the relationship between the LTC, the number of supercells, and the magnitude of atomic displacements in the wurtzite-type ZnS. The DFT calculation is used to determine the equilibrium structure of the wurtzite structure, but residual forces still remain in the equilibrium structure within a given convergence crite-

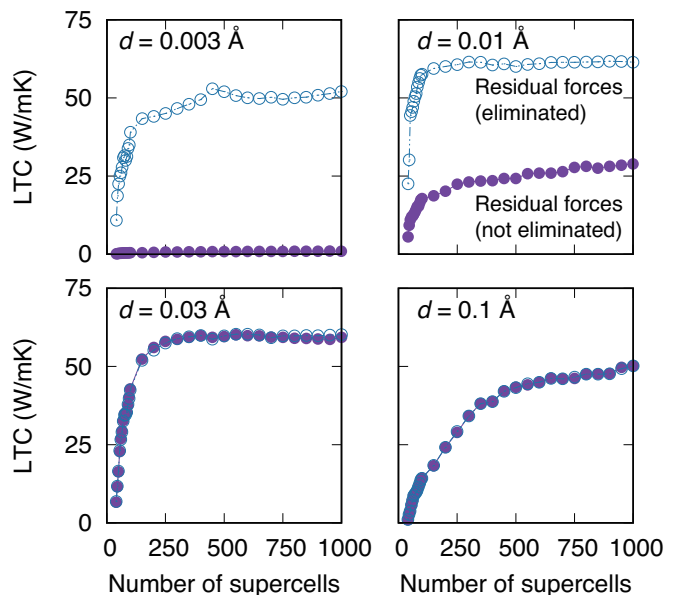


FIG. 7. Convergence behavior of LTC with respect to the number of supercells in the wurtzite-type ZnS. Displacement-force datasets are developed using only the DFT calculation. The supercell size is $3 \times 3 \times 2$, and the minimum number of supercells required for constructing a full-rank predictor matrix is 36. The average values of diagonal elements in LTC tensors are shown. The LTC values calculated using the forces from which the residual forces are not subtracted are represented by the closed circles, while the LTC values calculated using the forces where the residual forces are eliminated are represented by the open circles.

rion. These residual forces become a source of errors in the forces and can have a significant impact on the prediction of the LTC, particularly when the magnitudes of atomic displacements and forces are small. In the case of using $d = 0.003$ and 0.01 Å, the LTC values are sensitive to whether or not the residual forces are subtracted from the DFT values of the forces in supercell structures, as seen in Fig. 7. On the other hand, the magnitudes of the forces in supercell structures with $d = 0.03$ and 0.1 Å are large enough that the LTC values are independent of the subtraction of residual forces.

From the results in Fig. 7, it is clear that subtracting residual forces is essential for estimating force constants and LTCs precisely and robustly. However, when using $d = 0.003$ Å, the converged LTC value is slightly different from those for $d = 0.01$ and 0.03 Å. This difference may arise from the fact that the residual forces and other numerical errors in the DFT calculation are too large to estimate the LTC precisely. On the other hand, when using $d = 0.1$ Å, higher-order contributions are significant, and their truncation causes the slow convergence of the LTC with respect to the number of supercells. Therefore, it is recommended that the magnitude of atomic displacements is set between $d = 0.01$ and 0.03 Å in this case.

In comparison to the diamond structure, a greater

number of supercell structures are needed due to the increase of basis vectors for the force constants. In such a case, it is beneficial to adopt a more efficient approach for determining the force constants [38]. In this approach, the current projector-based procedure is combined with the use of on-the-fly MLPs, which are developed from the displacement-force dataset. This approach can significantly reduce the number of supercell structures required for the DFT calculation. At the same time, the force constants and LTCs can be predicted as accurately as those calculated from DFT calculations for a much larger number of structures.

VI. CONCLUSION

In this study, we have proposed a projector-based approach to efficiently build a complete orthonormal basis set for the second-order and third-order force constants. We have introduced several compression techniques that enable the reduction of the basis set in an efficient manner. These techniques compress a projection matrix using eigenvectors of another projection matrix onto subspaces defined by partial requirements for the force constants. Our efficient procedures for the basis-set construction and force constant estimation from a displacement-force dataset are implemented in the symfc code [1]. Additionally, extending this approach to higher-order force constants may be straightforward.

The obtained basis set satisfies all the necessary requirements for the force constants, including the permutation symmetry rules, sum rules, and symmetric properties required by the space group operations of the target structure. Therefore, the complete orthonormal basis set helps efficiently obtain precise force constants that exactly satisfy constraints on the force constants. As a result, properties related to the force constants, such as LTCs, can be precisely and efficiently calculated using the basis set for the force constants, as demonstrated in the applications of this study.

ACKNOWLEDGMENTS

This work was supported by JSPS KAKENHI Grant Numbers JP22H01756, and JP19H05787, and JP21K04632.

Appendix A: Computational efficiency

In this section, we present benchmark results that demonstrate the computational efficiency of generating force-constant basis sets and computing force constants from displacement-force datasets. Figure 8 shows the elapsed time required for computing the basis set of second-order and third-order supercell force constants for elemental and ionic structures. The computational cost

mainly depends on the number of atoms in the supercell because the numbers of second-order and third-order force-constant elements increase as $9N^2$ and $27N^3$, respectively. Moreover, the computational cost also varies depending on the symmetry of the target structure. Structures with lower symmetry tend to require a higher computational cost than those with higher symmetry, since their symmetric properties can efficiently reduce basis sets. This is ascribed to the fact that it is more computationally demanding to solve the compressed eigenvalue problem given by Eq. (59) in the former.

Then, we have conducted a benchmark to estimate force constants from displacement-force datasets in diamond Si. Figure 9 (a) shows the elapsed time and peak memory usage in estimating force constants with different subset sizes. For this benchmark, we use a dataset comprising 3000 structures with a supercell size of $3 \times 3 \times 3$ in diamond Si. As shown in Fig. 9 (a), the computational cost does not depend on the subset size of up to 400 structures, while the required memory size is almost proportional to the subset size. Therefore, we suggest that the subset size should not exceed 100.

Figure 9 (b) shows the elapsed time and peak memory usage in estimating force constants with a fixed subset size of 100, but with different numbers of supercells. The computational cost is proportional to the number of supercells in the dataset, while the required memory size remains almost constant, irrespective of the number of supercells. This result indicates that the subset division of $\mathbf{X}^\top \mathbf{X}$ is effective in reducing memory consumption.

Finally, in Fig. 9 (c), we present the elapsed time and peak memory usage in estimating force constants with a fixed subset size of 100 and a fixed number of supercells of 3000. We use three supercell sizes of $2 \times 2 \times 2$, $3 \times 3 \times 3$, and $4 \times 4 \times 4$ for the benchmark. The results indicate that the computational cost and the required memory size strongly depend on the number of atoms in the supercell.

Appendix B: Commutation relations of projection matrices

In this section, we present a proof of the commutation relations between projection matrices, $[\mathbf{P}_{\text{spg}}, \mathbf{P}_v] = 0$ and $[\mathbf{P}_{\text{spg}}, \mathbf{P}_w] = 0$. Although we only provide a proof for the second-order force constants, it can easily be extended to the third-order force constants. Suppose we have two orthogonal projection matrices, \mathbf{P}_1 and \mathbf{P}_2 . Therefore, the transpose of the product of \mathbf{P}_1 and \mathbf{P}_2 is given by $(\mathbf{P}_1 \mathbf{P}_2)^\top = \mathbf{P}_2^\top \mathbf{P}_1^\top = \mathbf{P}_2 \mathbf{P}_1$. If $\mathbf{P}_1 \mathbf{P}_2$ is symmetric, i.e., $\mathbf{P}_1 \mathbf{P}_2 = (\mathbf{P}_1 \mathbf{P}_2)^\top$, then \mathbf{P}_1 and \mathbf{P}_2 commute. In the following, we will demonstrate that the product of two projection matrices is symmetric.

(1) Proof of $[\mathbf{P}_{\text{spg}}, \mathbf{P}_v] = 0$. Firstly, we will show that $\mathbf{P}_v \mathbf{P}_{\text{spg}}$ is symmetric, $\mathbf{P}_v \mathbf{P}_{\text{spg}} = (\mathbf{P}_v \mathbf{P}_{\text{spg}})^\top$. Since the projection matrix \mathbf{P}_v is given by $\mathbf{P}_v = \mathbf{I} - \mathbf{C}_v \mathbf{C}_v^\top$ as shown in Eq. (22), the elements of $\mathbf{P}_v^c = \mathbf{C}_v \mathbf{C}_v^\top$ are

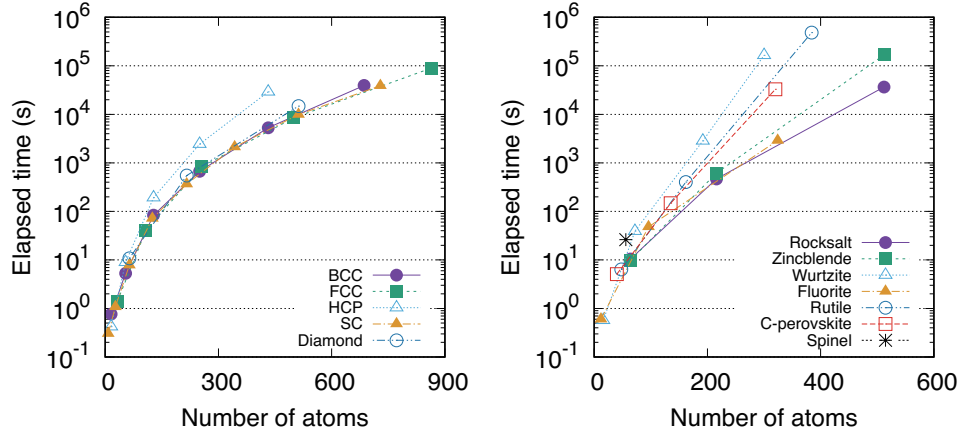


FIG. 8. Elapsed time required for computing basis sets for elemental and ionic structures. The elapsed times are measured using Intel(R) Xeon(R) CPU E5-2683 v4.

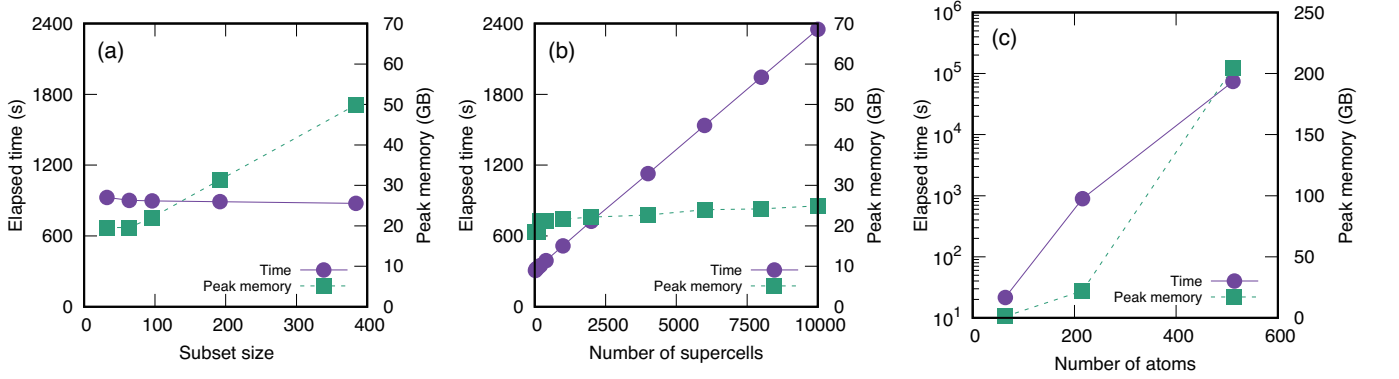


FIG. 9. (a) Elapsed time and peak memory usage in estimating force constants with different subset sizes in diamond Si. The number of supercells, the supercell size, and the magnitude of atomic displacements are 3000, $3 \times 3 \times 3$ (216 atoms), and $d = 0.001 \text{ \AA}$, respectively. (b) Elapsed time and peak memory usage in estimating force constants with a fixed subset size of 100 and different numbers of supercells in diamond Si. The subset size, the supercell size, and the magnitude of atomic displacements are 3000, $3 \times 3 \times 3$ (216 atoms), and $d = 0.001 \text{ \AA}$, respectively. (c) Elapsed time and peak memory usage in estimating force constants with a fixed subset size of 100 and a fixed number of supercells of 3000. The magnitude of atomic displacements is set to $d = 0.001 \text{ \AA}$. The elapsed times are measured using Intel(R) Xeon(R) CPU E5-2683 v4.

expressed as

$$P_{v,(i\alpha j\beta,i'\alpha'j'\beta')}^c = \frac{1}{N} \delta_{ii'} \delta_{\alpha\alpha'} \delta_{\beta\beta'}, \quad (\text{B1})$$

where $\delta_{ii'}$ denotes the Kronecker delta. Therefore, when denoting the product of \mathbf{P}_v^c and \mathbf{P}_{spg} as $\mathbf{P}' = \mathbf{P}_v^c \mathbf{P}_{\text{spg}}$, its elements are written as

$$\begin{aligned} P'_{(i\alpha j\beta,i'\alpha'j'\beta')} &= \sum_{k\gamma l\delta} P_{v,(i\alpha j\beta,k\gamma l\delta)}^c P_{\text{spg}(k\gamma l\delta,i'\alpha'j'\beta')} \\ &= \frac{1}{N} \sum_l P_{\text{spg}(i\alpha l\beta,i'\alpha'j'\beta')} \end{aligned} \quad (\text{B2})$$

and

$$\begin{aligned} P'_{(i'\alpha'j'\beta',i\alpha j\beta)} &= \sum_{k\gamma l\delta} P_{v,(i'\alpha'j'\beta',k\gamma l\delta)}^c P_{\text{spg}(k\gamma l\delta,i\alpha j\beta)} \\ &= \frac{1}{N} \sum_l P_{\text{spg}(i'\alpha'l\beta',i\alpha j\beta)} \\ &= \frac{1}{N} \sum_l P_{\text{spg}(i\alpha j\beta,i'\alpha'l\beta')}. \end{aligned} \quad (\text{B3})$$

The final equality is derived from the symmetric property of \mathbf{P}_{spg} . Using the definition of \mathbf{P}_{spg} , these elements are expressed as

$$\begin{aligned} P'_{(i\alpha j\beta,i'\alpha'j'\beta')} &= \frac{1}{N|\mathcal{G}|} \sum_l \sum_{\hat{g} \in \mathcal{G}} \Gamma(\hat{g})_{(i\alpha,i'\alpha')} \Gamma(\hat{g})_{(l\beta,j'\beta')} \end{aligned} \quad (\text{B4})$$

and

$$\begin{aligned} & P'_{(i'\alpha'j'\beta',i\alpha j\beta)} \\ &= \frac{1}{N|\mathcal{G}|} \sum_l \sum_{\hat{g} \in \mathcal{G}} \Gamma(\hat{g})_{(i\alpha,i'\alpha')} \Gamma(\hat{g})_{(j\beta,l\beta')}, \end{aligned} \quad (\text{B5})$$

respectively. The summations over index l in Eqs. (B4) and (B5) must then be equal, i.e.,

$$\sum_l \Gamma(\hat{g})_{(l\beta,j'\beta')} = \sum_l \Gamma(\hat{g})_{(j\beta,l\beta')}, \quad (\text{B6})$$

because $\Gamma(\hat{g})_{(l\beta,j'\beta')}$ can be non-zero only for single atom l such that operation \hat{g} moves atom l to atom j' and its value corresponds to the representation of \hat{g} for the Cartesian components (β, β') . When we denote these summations as $\Gamma'(\hat{g})_{(\beta, \beta')}$, the elements of \mathbf{P}' are written as

$$\begin{aligned} & P'_{(i\alpha j\beta, i'\alpha' j'\beta')} = P'_{(i'\alpha' j'\beta', i\alpha j\beta)} \\ &= \frac{1}{N|\mathcal{G}|} \sum_{\hat{g} \in \mathcal{G}} \Gamma(\hat{g})_{(i\alpha, i'\alpha')} \Gamma'(\hat{g})_{(\beta, \beta')}, \end{aligned} \quad (\text{B7})$$

which is equivalent to $\mathbf{P}_v^c \mathbf{P}_{\text{spg}} = (\mathbf{P}_v^c \mathbf{P}_{\text{spg}})^\top$. Therefore, $\mathbf{P}_v \mathbf{P}_{\text{spg}} = (\mathbf{P}_v \mathbf{P}_{\text{spg}})^\top$ can also be derived, and it has been proved that $[\mathbf{P}_{\text{spg}}, \mathbf{P}_v] = 0$.

(2) Proof of $[\mathbf{P}_{\text{spg}}, \mathbf{P}_w] = 0$. We demonstrate that $\mathbf{P}_w \mathbf{P}_{\text{spg}}$ is symmetric. The projection matrix \mathbf{P}_w is represented by $\mathbf{P}_w = \mathbf{B}_w \mathbf{B}_w^\top$. Therefore, the elements of matrix $\mathbf{P}'' = \mathbf{P}_w \mathbf{P}_{\text{spg}}$ are written as

$$P''_{(i\alpha j\beta, i'\alpha' j'\beta')} = \frac{1}{2} [P_{\text{spg}(i\alpha j\beta, i'\alpha' j'\beta')} + P_{\text{spg}(j\beta i\alpha, i'\alpha' j'\beta')}] \quad (\text{B8})$$

and

$$P''_{(i'\alpha' j'\beta', i\alpha j\beta)} = \frac{1}{2} [P_{\text{spg}(i'\alpha' j'\beta', i\alpha j\beta)} + P_{\text{spg}(j'\beta' i'\alpha', i\alpha j\beta)}]. \quad (\text{B9})$$

Then, the projection matrix \mathbf{P}_{spg} is orthogonal and has the following symmetric properties of

$$P_{\text{spg}(i\alpha j\beta, i'\alpha' j'\beta')} = P_{\text{spg}(i'\alpha' j'\beta', i\alpha j\beta)} \quad (\text{B10})$$

and

$$\begin{aligned} P_{\text{spg}(j\beta i\alpha, i'\alpha' j'\beta')} &= P_{\text{spg}(i'\alpha' j'\beta', j\beta i\alpha)} \\ &= P_{\text{spg}(j'\beta' i'\alpha', i\alpha j\beta)}, \end{aligned} \quad (\text{B11})$$

where the final equality is derived from the fact that \mathbf{P}_{spg} is expressed as the sum of the Kronecker products of representation $\mathbf{\Gamma}(\hat{R})$. After applying these equations, we can conclude that \mathbf{P}'' is symmetric as

$$P''_{(i\alpha j\beta, i'\alpha' j'\beta')} = P''_{(i'\alpha' j'\beta', i\alpha j\beta)}, \quad (\text{B12})$$

which proves that $[\mathbf{P}_{\text{spg}}, \mathbf{P}_w] = 0$.

Appendix C: Efficient implementation of force-constant estimation

When dividing the displacement-force dataset, we adopt the following procedure to compute $\mathbf{X}^\top \mathbf{X}$ and $\mathbf{X}^\top \mathbf{y}$ more efficiently. Introducing variables $z_{i\alpha, c}^{(s, \text{FC2})}$ and $z_{i\alpha, c}^{(s, \text{FC3})}$ defined by

$$\begin{aligned} z_{i\alpha, c}^{(s, \text{FC2})} &= -\sum_{j\beta} u_{j\beta}^{(s)} C_{i\alpha, j\beta, c}^{(\text{FC2})} \\ z_{i\alpha, c}^{(s, \text{FC3})} &= -\frac{1}{2} \sum_{j\beta} \sum_{k\gamma} u_{j\beta}^{(s)} u_{k\gamma}^{(s)} C_{i\alpha, j\beta, k\gamma, c}^{(\text{FC3})}, \end{aligned} \quad (\text{C1})$$

the forces acting on atoms in supercell structure s is rewritten by

$$\begin{aligned} f_{i\alpha}^{(s)} &= \sum_b w_b^{(\text{FC2})} \sum_c z_{i\alpha, c}^{(s, \text{FC2})} E_{c, b}^{(\text{FC2})} \\ &+ \sum_b w_b^{(\text{FC3})} \sum_c z_{i\alpha, c}^{(s, \text{FC3})} E_{c, b}^{(\text{FC3})}. \end{aligned} \quad (\text{C2})$$

In a matrix form, the forces are represented as

$$\begin{aligned} \mathbf{f}^{(s)} &= \mathbf{Z}^{(s)} \mathbf{E} \mathbf{w} \\ &= \mathbf{X}^{(s)} \mathbf{w}, \end{aligned} \quad (\text{C3})$$

where

$$\begin{aligned} \mathbf{Z}^{(s)} &= [\mathbf{Z}^{(s, \text{FC2})} \quad \mathbf{Z}^{(s, \text{FC3})}] \\ &= \begin{bmatrix} \dots & \vdots & \dots & \vdots & \dots \\ \dots & z_{i\alpha, c}^{(s, \text{FC2})} & \dots & z_{i\alpha, c}^{(s, \text{FC3})} & \dots \\ \dots & \vdots & \dots & \vdots & \dots \end{bmatrix}, \end{aligned} \quad (\text{C4})$$

and

$$\mathbf{E} = \begin{bmatrix} \mathbf{E}^{(\text{FC2})} & \mathbf{0} \\ \mathbf{0} & \mathbf{E}^{(\text{FC3})} \end{bmatrix}. \quad (\text{C5})$$

For the displacement-force dataset, matrix \mathbf{Z} is expressed as

$$\begin{aligned} \mathbf{Z} &= \begin{bmatrix} \mathbf{Z}^{(1)} \\ \mathbf{Z}^{(2)} \\ \mathbf{Z}^{(3)} \\ \vdots \\ \mathbf{Z}^{(N_s)} \end{bmatrix} = \begin{bmatrix} \mathbf{Z}^{(1, \text{FC2})} & \mathbf{Z}^{(1, \text{FC3})} \\ \mathbf{Z}^{(2, \text{FC2})} & \mathbf{Z}^{(2, \text{FC3})} \\ \mathbf{Z}^{(3, \text{FC2})} & \mathbf{Z}^{(3, \text{FC3})} \\ \vdots & \vdots \\ \mathbf{Z}^{(N_s, \text{FC2})} & \mathbf{Z}^{(N_s, \text{FC3})} \end{bmatrix} \\ &= [\mathbf{Z}^{(\text{FC2})} \quad \mathbf{Z}^{(\text{FC3})}]. \end{aligned} \quad (\text{C6})$$

Using these representations, $\mathbf{X}^\top \mathbf{X}$ and $\mathbf{X}^\top \mathbf{y}$ can be rewritten as

$$\mathbf{X}^\top \mathbf{X} = \mathbf{E}^\top \mathbf{Z}^\top \mathbf{Z} \mathbf{E} = \begin{bmatrix} \mathbf{E}^{(\text{FC2})\top} \mathbf{Z}^{(\text{FC2})\top} \mathbf{Z}^{(\text{FC2})} \mathbf{E}^{(\text{FC2})} & \mathbf{E}^{(\text{FC2})\top} \mathbf{Z}^{(\text{FC2})\top} \mathbf{Z}^{(\text{FC3})} \mathbf{E}^{(\text{FC3})} \\ \mathbf{E}^{(\text{FC3})\top} \mathbf{Z}^{(\text{FC3})\top} \mathbf{Z}^{(\text{FC2})} \mathbf{E}^{(\text{FC2})} & \mathbf{E}^{(\text{FC3})\top} \mathbf{Z}^{(\text{FC3})\top} \mathbf{Z}^{(\text{FC3})} \mathbf{E}^{(\text{FC3})} \end{bmatrix}, \quad (\text{C7})$$

and

$$\mathbf{X}^\top \mathbf{y} = \mathbf{E}^\top \mathbf{Z}^\top \mathbf{y} = \begin{bmatrix} \mathbf{E}^{(\text{FC2})\top} \mathbf{Z}^{(\text{FC2})\top} \mathbf{y} \\ \mathbf{E}^{(\text{FC3})\top} \mathbf{Z}^{(\text{FC3})\top} \mathbf{y} \end{bmatrix}, \quad (\text{C8})$$

respectively. Finally, the matrix products with forms of $\mathbf{Z}^\top \mathbf{Z}$ and $\mathbf{Z}^\top \mathbf{y}$ are calculated efficiently by dividing \mathbf{Z} and \mathbf{y} into subsets.

- [1] A. Seko and A. Togo, “Symfc,” <https://github.com/symfc/symfc>.
- [2] M. T. Dove, *Introduction to Lattice Dynamics* (Cambridge University Press, 1993).
- [3] D. C. Wallace, *Thermodynamics of crystals* (Dover Publications, 1998).
- [4] J. M. Ziman, *Electrons and phonons: the theory of transport phenomena in solids* (Oxford University Press, 1960).
- [5] K. Parlinski, Z. Q. Li, and Y. Kawazoe, Phys. Rev. Lett. **78**, 4063 (1997).
- [6] O. Hellman, P. Steneteg, I. A. Abrikosov, and S. I. Simak, Phys. Rev. B **87**, 104111 (2013).
- [7] T. Tadano and S. Tsuneyuki, J. Phys. Soc. Jpn. **87**, 041015 (2018).
- [8] F. Eriksson, E. Fransson, and P. Erhart, Adv. Theory Simul. **2**, 1800184 (2019).
- [9] A. Togo, J. Phys. Soc. Jpn. **92**, 012001 (2023).
- [10] I. Errea, M. Calandra, and F. Mauri, Phys. Rev. Lett. **111**, 177002 (2013).
- [11] A. van Roekeghem, J. Carrete, and N. Mingo, Comput. Phys. Commun. **263**, 107945 (2021).
- [12] J. F. Nye, *Physical Properties of Crystals* (Oxford University Press, 1985).
- [13] M. El-Batanouny and F. Wooten, *Symmetry and Condensed Matter Physics: A Computational Approach* (Cambridge University Press, 2008).
- [14] G. Venkataraman, L. A. Feldkamp, and V. C. Sahni, *Dynamics of perfect crystals* (MIT press, 1975).
- [15] F. Zhou, W. Nielson, Y. Xia, and V. Ozoliņš, Phys. Rev. Lett. **113**, 185501 (2014).
- [16] T. Tadano and S. Tsuneyuki, Phys. Rev. B **92**, 054301 (2015).
- [17] H. Yanai, K. Takeuchi, and Y. Takane, *Projection Matrices, Generalized Inverse Matrices, and Singular Value Decomposition*, Statistics for social and behavioral sciences (Springer, Dordrecht, 2011).
- [18] G. Strang, *Introduction to Linear Algebra*, 6th ed. (CUP, 2023).
- [19] R. Piziak, P. Odell, and R. Hahn, Comput. Math. Appl. **37**, 67 (1999).
- [20] J. von Neumann, Annals of Math. **50**, 401 (1949).
- [21] I. Halperin, Acta Sci. Math.(Szeged) **23**, 96 (1962).
- [22] A. Galántai, *Projectors and projection methods*, Vol. 6 (Springer Science & Business Media, 2013).
- [23] R. Sedgewick, *Algorithms in c, part 5: graph algorithms, third edition*, 3rd ed. (Addison-Wesley Professional, 2001).
- [24] A. Seko, A. Togo, and I. Tanaka, Phys. Rev. B **99**, 214108 (2019).
- [25] A. Seko, J. Appl. Phys. **133**, 011101 (2023).
- [26] P. E. Blöchl, Phys. Rev. B **50**, 17953 (1994).
- [27] J. P. Perdew, K. Burke, and M. Ernzerhof, Phys. Rev. Lett. **77**, 3865 (1996).
- [28] G. Kresse and J. Hafner, Phys. Rev. B **47**, 558 (1993).
- [29] G. Kresse and J. Furthmüller, Phys. Rev. B **54**, 11169 (1996).
- [30] G. Kresse and D. Joubert, Phys. Rev. B **59**, 1758 (1999).
- [31] R. E. Peierls, Ann. Phys. **395**, 1055 (1929).
- [32] R. E. Peierls, *Quantum theory of solids* (Oxford University Press, 2001).
- [33] P. B. Allen and V. Perebeinos, Phys. Rev. B **98**, 085427 (2018).
- [34] A. Togo, L. Chaput, and I. Tanaka, Phys. Rev. B **91**, 094306 (2015).
- [35] A. Togo, L. Chaput, T. Tadano, and I. Tanaka, J. Phys. Condens. Matter **35**, 353001 (2023).
- [36] S. Fujii and A. Seko, Comput. Mater. Sci. **204**, 111137 (2022).
- [37] A. Seko, Polynomial Machine Learning Potential Repository at Kyoto University, <https://sekocha.github.io>.
- [38] A. Togo and A. Seko, arXiv preprint arXiv:2401.17531 (2024).